IEEE Access
Multidisciplinary | Rapid Review | Open Access Journal

Received 4 October 2022, accepted 28 October 2022, date of publication 7 November 2022, date of current version 16 November 2022.

Digital Object Identifier 10.1109/ACCESS.2022.3220223

RESEARCH ARTICLE

A Study on Control Strategies for Aggregated Community Energy Storage Systems in Medium Voltage Distribution Networks

HERNÁN YEPES-FERNÁNDEZ, (Student Member, IEEE), MAURICIO RESTREPO, (Member, IEEE), AND ADRIANA ARANGO-MANRIQUE, (Member, IEEE)
Department of Electrical and Electronic Engineering, Universidad del Norte, Barranquilla 081007, Colombia
Corresponding author: Mauricio Restrepo (mauriciorestrepo@uninorte.edu.co)

This work was supported by Universidad del Norte through Internal Research Agendas Program.

ABSTRACT Community Energy Storage Systems (CESSs) emerge as an innovative way to integrate batteries into Low Voltage (LV) and Medium Voltage (MV) distribution networks to provide ancillary services and improve the quality of energy received by the end user. However, since CESSs are still emerging technologies, there is much research space in this field for proposing innovative and economic control algorithms for such devices. Thus, this paper presents a study of four control strategies applied to an MV distribution network, i.e., peak shaving, line losses control, line congestion reduction, and system voltage control, through an Aggregated Community Energy Storage System (ACESS), which is represented as the sum of multiple CESSs connected in LV systems, viewed from MV side. The proposed strategies are based on Model Predictive Control (MPC), a technique that, using the future demand forecast data, calculates the dispatch of ACESS. The results show, with respect to the base case, an improvement between 12.8% and 15.1% for the line losses control strategy, a reduction of 31.5% on the maximum demand for the peak shaving control strategy, a maximum lowering of 12% on the currents of some lines for the congestion control strategy, and an enhancement of 0.15% for the voltage control strategy. Moreover, for estimating the service lifetime of the ACESS after applying the control algorithms, the Rainflow Counting Algorithm (RCA) is used, exhibiting that, regardless of the control strategy, the degradation is inversely proportional to the storage capacity.

INDEX TERMS Ancillary services, batteries, community energy storage systems (CESSs), degradation, model predictive control (MPC).

NOMENCLATURE

Acronyms

BESS	Battery Energy Storage System.
CESS	Community Energy Storage System.
DoD	Depth of Discharge.
ESS	Energy Storage System.
LV	Low Voltage.
MPC	Model Predictive Control.
MV	Medium Voltage.
OPF	Optimal Power Flow.
PV	Photovoltaic.
RCA	Rainflow Counting Algorithm.
SoC	State of Charge.

Sub- and Super-Indices

bat	Battery.
c	Charge.
d	Discharge.
DoD	Depth of discharge.
G	Generated energy.
grid	Network equivalent.
j	Control strategy equation weight index.
k	Time step.

The associate editor coordinating the review of this manuscript and approving it for publication was Yongquan Sun.

L	Consumed energy.
m	Limit iteration index.
net	Energy grid and energy battery difference.
psl	Peak shaving limit.
SoC	State of charge.

Parameters

Δt	Time difference between iterations.
η_c	Charge efficiency.
η_d	Discharge efficiency.
a	Control strategy equation weight.
A_c, A_d, a_c, a_d, a_i	Weight matrices of DoD calculation.
C	Iteration counter limit.
Cap	CESS capacity.
$Load$	System load.
u_{bat}^{max}	Maximum battery output or input.
u_{grid}^{max}	Maximum grid output.

Variables

L	Grid participation limit.
u^{bat}	Battery power.
u^{grid}	Grid power.
u^{net}	Grid and Load power difference.
x^{DoD}	DoD value.
x^{SoC}	SoC value.

I. INTRODUCTION

Battery Energy Storage Systems (BESSs) are emerging as a solution to multiple problems within electric power systems. They offer great flexibility, provide numerous applications in the form of ancillary services, and serve as an interface for various renewable generation technologies. Community Energy Storage Systems (CESSs) appear as part of this group of distributed energy resources, being a set of variable storage capacity BESSs and an inverter that are installed near a group of end users [1], [2], [3]. This characteristic implies, among other things, that its applications are restricted to Medium Voltage (MV) and, more commonly, Low Voltage (LV) grids [4]. Additionaly, advances in research, development, and production of lithium-ion batteries have allowed a significant decrease in acquisition cost for CESS. According to EIA, the cost per kWh between 2015 and 2019 went from $20,000 USD to approximately $500 USD [5]. These figures indicate that CESSs may represent a cost-effective opportunity for improving the operation of MV and LV distribution systems.

The cost reduction in lithium-ion batteries has allowed the introduction of the Aggregated Community Energy Storage Systems (ACESSs), whose function is to combine and coordinate multiple CESS working on LV networks to improve the performance of the upstream MV systems. This allows the existence of groups of CESS that, summed up, reach capacities of the order of MWh of storage capacity that are able to provide multiple ancillary services in distribution systems [6]. However, very few applications found in the literature for CESS consider the figure of the aggregator, and most of the proposed solutions with CESS are focused on peak shaving algorithms for household loads in LV networks. Hence, there is an opportunity to evaluate different control strategies for providing ancillary services with ACESSs in MV distribution networks, focused on other phenomena such as losses, line congestion or voltage deviations.

The ancillary services that can be provided by ACESSs, and more generally by Battery Energy Storage Systems (BESSs), can be divided into energy applications and power applications. The former contains services such as energy arbitrage, renewable energy time shift, demand charge reduction, time of use charge reduction, transmission and distribution upgrade deferral, and grid resiliency, and the latter considers the provision of frequency regulation, voltage support, damping of power system oscillations, synthetic inertia, and ramp rate control in renewable sources [7]. Each of these applications requires a different control strategy; however, most of the control strategies applied to BESS aim to control the delivery and consumption of active and reactive power through the inverter connected to the grid. Additionally, it is also possible to classify the control strategies with BESSs based on the size of the storage system in MWh, the required discharge duration, the charging and discharging cycles of the storage system, and the required response time to execute the control action [8].

With respect to energy applications, an example of a peak shaving strategy, based on Model Predictive Control and focused on reducing the degradation of the BESS, is proposed in [9]. This strategy solves the dispatch of a battery during a 48-hour period in a single-node system with a network equivalent, a variable load, a Photovoltaic (PV) generation system and a BESS. The constraints associated with the dispatch are the balancing condition, i.e., that all the power consumed is equal to all the power delivered, and the grid participation limit, i.e., above a certain limit, the energy demanded by the load must be supplied by a BESS or a PV generator. The rest of the constraints are directly associated with the behavior of the BESS within the system, e.gr., the lower and upper limits of the SoC, or the maximum power deliverable by the batteries. The results obtained are satisfactory for the configured test system; however, this model can be improved for applications in three-phase, multi-node systems using complementary control strategies with MPC. Another example of peak shaving is found in [10], where multiple control strategies (losses control, peak shaving, voltage regulation, and reduction of the cost of implementation and maintenance of storage systems) are proposed and applied to a series of BESSs located along a power system. Even though the individual application of each of these control strategies works successfully, the paper proposes their joined application, without evaluating whether this improves their effectiveness or reduces their computational cost for real-time operation.

Among control strategies proposed for congestion reduction in power systems using BESS, [11] and [12] describe the reduction of congestion in lines with two different control strategies. In [11], the aim is to find an optimal economic dispatch for the BESS taking into account PV generation systems with stochastic behavior, achieving the reduction of line losses and congestion. In [12], the control strategy calculates the optimal dispatch of the generation and BESS units, considering the maximum power transfer and the thermal limits of the lines as constraints. In both [11] and [12], the results are based on a single power flow for a modified test system (IEEE 24-bus and 30-bus test systems), which leaves out the variability of loads throughout the day, making it impossible for the algorithms to prevent future variations. Moreover, authors in [13] propose a control strategy to reduce line losses and improve the voltage profile of a distribution system using an Optimal Power Flow (OPF) and testing the BESS at the end of a radial distribution network. The results only show a scenario of a single power flow in which a significant decrease in losses is observed; however, this paper makes no attempt to test other load conditions that may occur throughout the day, and other configuration such as non-radial systems.

Several works describe control strategies for power applications using BESSs. A first example is presented in [14]., where a voltage control scheme is performed at a multi-node, three-phase system using a series of PQ curves to estimate the DC voltage at the battery output, taking into account measurements of grid parameters, State of Charge (SoC), and battery terminal voltage at each time step. Based on these PQ curves, the algorithm decides how to correct under- and over-voltages within the grid using BESSs. However, this strategy is limited by the number of PQ curves that are initially loaded into the algorithm, reducing its effectiveness. Another voltage control scheme is described in [15], where a consesus algorithm is implemented for distributed BESSs connected to a distribution network. This method assigns weights to the existing connections among nodes to share the participation of each BESS in reducing or increasing the voltage at each node as required at each time step. Although this approach presents satisfactory results for compensating over- and under-voltages in a wide variety of scenarios, it might be expensive as it requires a large communication system for BESS coordination in real-time applications.

Most of the aforementioned solutions are applied without taking into account future load variations, so that the input data do not include the demand forecast, i.e., their input is fed only by the present and past variables of the system. Therefore, the main contribution of this work is the modification of the MPC presented in [9], by proposing four control strategies for ACESSs, i.e., peak shaving, line loss reduction, voltage control and line congestion reduction. At each 15-min time step over a 24-h horizon, the MPC strategy performs the dispatch of an ACESS connected to a three-phase multi-node system, which is obtained by adding a future demand forecast that allows estimating whether the battery will need to be charged or discharged before peak demand arrives, as compared to the initial model that was intended for a single-node and single-phase system. Also, according to the selected control strategy, some constraints are added to the MPC approach. Finally, the degradation suffered by multiple size ACESSs is estimated through a Rainflow Counting Algorithm (RCA) whose input is the resulting SoC from each dispatch.

The rest of this paper is organized as follows: Section II presents the methodology and describes the proposed MPC algorithm with ACESSs, and Section III discusses the implementation of the models and describes the case studies. Then, Section IV provides the results for each case study and control strategies, as well as a discussion of the results. Finally, Section V shows the conclusions of this work.

II. METHODOLOGY

The proposed algorithm, whose operation is depicted in Fig. 1, is responsible of performing the ACESS dispatch in order to provide simultaneously peak shaving and other services such as voltage control, line losses reduction, and congestion control in a distribution system.

Figure 1 is divided into 5 boxes that describe each processing stage of the proposed method. Box 1 shows the external packages that are necessary for coding and operating the MPC algorithm in Python. These are Pyomo [16], which is an optimization modeling language; Matplotlib, for plotting results; and Pandas, for importing and exporting information from and to files in.csv, .xls or .xlsx format. Box 2 indicates the actions that need to be performed according to the iteration number, i.e., if zero, the algorithm creates the optimization model for the new initial conditions, otherwise, it employs the result of the previous iteration as the initial value for the new step. Box 3 presents which control strategy will be applied among peak shaving, losses reduction, voltage control or congestion reduction, as explained later in Section II-A. Box 4 introduces the optimization problem that is solved using CPLEX [17], and how the results are plotted in the form of a forecast of the SoC and the corresponding power dispatch. Finally, box 5 describes how the initial variables of the next iteration are updated, and how the cycle is repeated unless the demand forecast data is finished, in which case, the algorithm finishes its run and exports all the information of the response variables that were calculated in each iteration.

A. MPC DISPATCH ALGORITHM

The MPC model described in [9] is characterized by having prediction and control horizons of 24 hours and 15 minutes, respectively, so that 72-hour forecast data with 15-minute steps is necessary for a 48-hour implementation of this algorithm, as seen in Fig. 6. Thus, the objective function and the constraints of the proposed MPC model for ACESS, modified from [9], are described as follows:

- Objective function: The objective function described in (1) is a quadratic cost function aimed to minimize the

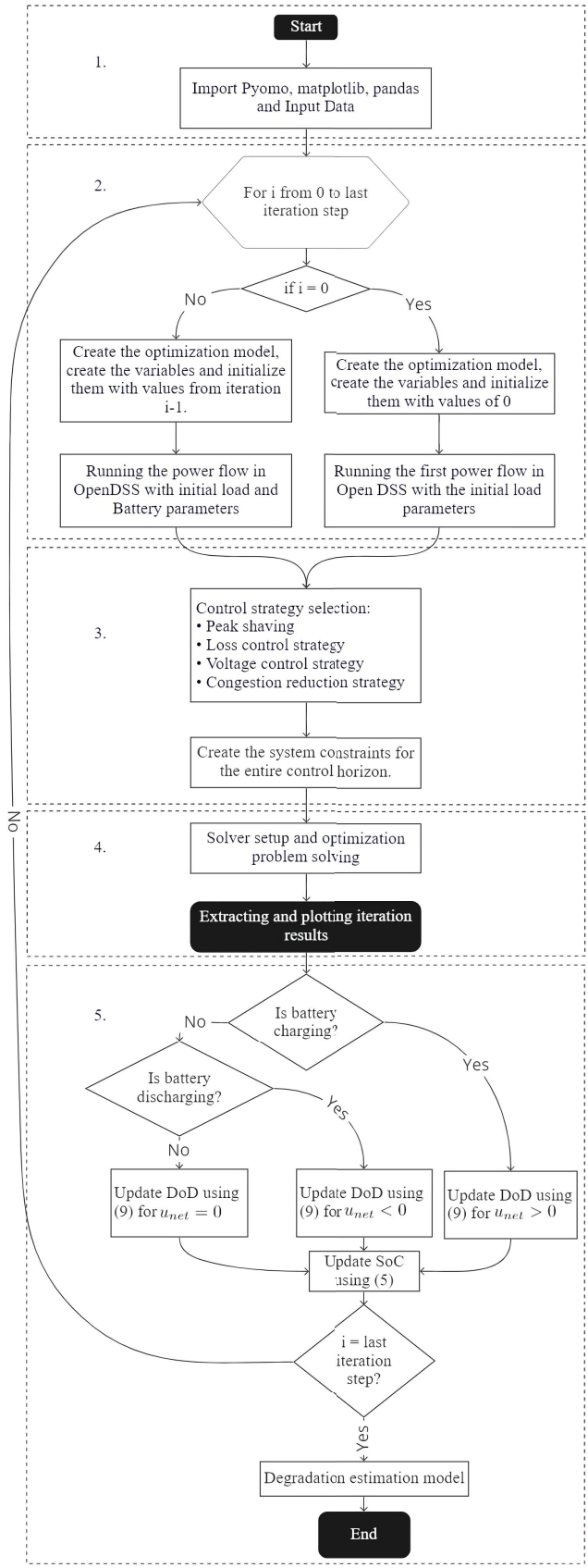

FIGURE 1. Flowchart of the proposed ACESS control algorithm.

participation of ACESS in the system dispatch, by keeping the SoC as close as possible to a reference value of 0.45 because, according to [9], it is the point of minimum degradation induced to a BESS at idle state. Then, the objective function consists of the summation of costs associated to charging and discharging Depth of Discharge (DoD), u^{bat}, charging and discharging commitment, and CESS SoC. The particular cost coefficients associated to each of these variables are extracted from [9].

$$z = \sum_{k=1}^{96}[(1.6x_k^{DoD,c})^2 + 1.2 * 10^{-7}(x_k^{DoD,d})^2 + 1.2 * 10^{-7}\,(u_k^{bat,c})^2 + 1.6(u_k^{bat,d})^2 + 2 * ((x_k^{SoC})^2 - 0.9 * (x_k^{SoC}) + 0.45^2)] \quad (1)$$

- Power balance: Equation (2) describes the power balance conditions between generation and demand for each time step. Note in (3)-(4) that, depending of the charge or discharge phase of the battery, the corresponding power will be seen in the equation as a load or a generator

$$\sum u_k^G - \sum u_k^L = 0 \;\; \forall k \in \{1, \ldots, 96\} \quad (2)$$

$$u_k^G = u_k^{bat,d} + u_k^{grid} \;\; \forall k \in \{1, \ldots, 96\} \quad (3)$$

$$u_k^L = Load_k + u_k^{bat,c} \;\; \forall k \in \{1, \ldots, 96\} \quad (4)$$

- Battery constraints: These constraints are divided into SoC constraints and DoD constraints. The former comprises (5) to (7), which describe the SoC calculation and its limits, and the latter includes (8) to (9), which define the corresponding DoD depending on the CESS charging or discharging.

$$x_{k+1}^{SoC} = x_k^{SoC} + \Delta x_{k+1}^{SoC} \;\; \forall k = \{1, \ldots, 95\} \quad (5)$$

$$\Delta x_{k+1}^{SoC} = \frac{\Delta t(\eta_L u_k^L - \eta_G^{-1} u_k^G)}{Cap} \;\; \forall k = \{1, \ldots, 95\} \quad (6)$$

SoC lower and upper limits, depicted in (7), are defined as 0.2 and 0.85 as per in [18] and [19] since these are typical values considered in practical applications that guarantee a safe battery operation.

$$0.2 \leq x_k^{SoC} \leq 0.85 \;\; \forall k = \{1, \ldots, 96\} \quad (7)$$

DoD is estimated in (8) and (9) as a piecewise-linear function that depends on SoC and DoD, according to the case selected in box 5 of Fig.1. In these equations, the parameters A_c, A_d, a_c, a_d, and a_i are weight matrices that serve to estimate the next value of the DoD, as described in (9) and (9).

$$x_k^{DoD} = \begin{pmatrix} x_k^{DoD,c} \\ x_k^{DoD,d} \end{pmatrix} \;\; \forall k \in \{1, \ldots, 96\} \quad (8)$$

$$x_{k+1}^{DoD} = \begin{cases} A_c x_k^{DoD} + a_c \Delta x^{SoC}, & \forall u_{net} > 0 \\ A_d x_k^{DoD} - a_d \Delta x^{SoC}, & \forall u_{net} < 0 \\ a_i, & \forall u_{net} = 0 \end{cases}$$
$$\forall k = \{1, \ldots, 95\}$$
$$A_c = \begin{bmatrix} 1 & 0 \\ 0 & 0 \end{bmatrix}, \; A_d = \begin{bmatrix} 0 & 0 \\ 0 & 1 \end{bmatrix}$$
$$a_c = \begin{pmatrix} 1 \\ 0 \end{pmatrix}, \; a_d = \begin{pmatrix} 0 \\ 1 \end{pmatrix}, \; a_i = \begin{pmatrix} 0 \\ 0 \end{pmatrix} \quad (9)$$

Moreover, (10)-(13) represent the maximum charging and discharging power limits of the CESS, and (14) indicates the complementarity constraint that prevents the CESS from charging and discharging simultaneously.

$$u_k^{bat,d} \geq 0 \;\; \forall k = \{1, \ldots, 96\} \quad (10)$$
$$u_k^{bat,d} \leq u^{bat,max} \;\; \forall k = \{1, \ldots, 96\} \quad (11)$$
$$u_k^{bat,c} \leq 0 \;\; \forall k = \{1, \ldots, 96\} \quad (12)$$
$$u_k^{bat,c} \geq -u^{bat,max} \;\; \forall k = \{1, \ldots, 96\} \quad (13)$$
$$u_k^{bat,c} * u_k^{bat,d} = 0 \;\; \forall k = \{1, \ldots, 96\} \quad (14)$$

- Grid constraints: Finally, the constraints presented in (15)-(17) describe the behavior of the external network equivalent, including the net energy calculation, and energy limits for generation and loads.

$$u_k^{net} = u_k^{grid} - u_k^{L} \;\; \forall k = \{1, \ldots, 96\} \quad (15)$$
$$0 \leq u_k^{G,grid} \leq u^{grid,max} \;\; \forall k = \{1, \ldots, 96\} \quad (16)$$
$$0 \leq u_k^{L,bat} \leq u^{grid,max} \;\; \forall k = \{1, \ldots, 96\} \quad (17)$$

B. CESS CONTROL STRATEGIES

The following subsections describe the details of the four control strategies that can be selected for the ACESS, as indicated in box 3 of Fig. 1.

1) PEAK SHAVING CONTROL STRATEGY

The peak shaving control strategy is a variation of the general optimization problem explained in Section II-A. In this case, the main modification consists of adding constraints that impose a participation limits to the grid for both charging and discharging. Thus, if the load exceeds the discharge participation limit $L_{grid,d}$, the missing energy will be supplied by the ACESS, whereas if the demand is lower than the charging participation limit $L_{grid,c}$, and the ACESS can or requires to store energy, then it will be charged. Both charging and discharging constraints are defined in (18) and (19).

$$L_{grid,c} = L_{grid}^{psl} \quad (18)$$
$$L_{grid,d} = L_{grid}^{psl} \quad (19)$$

2) LINE LOSSES CONTROL STRATEGY

The line losses control strategy, depicted in Fig. 2, modifies the network participation constraints (18) and (19) through a parameter that describes the difference between the line losses in the base case without the ACESS and the losses with the ACESS installed, as per (20). This information is extracted directly from the power flow calculated in each iteration. When the losses remain the same or increase with

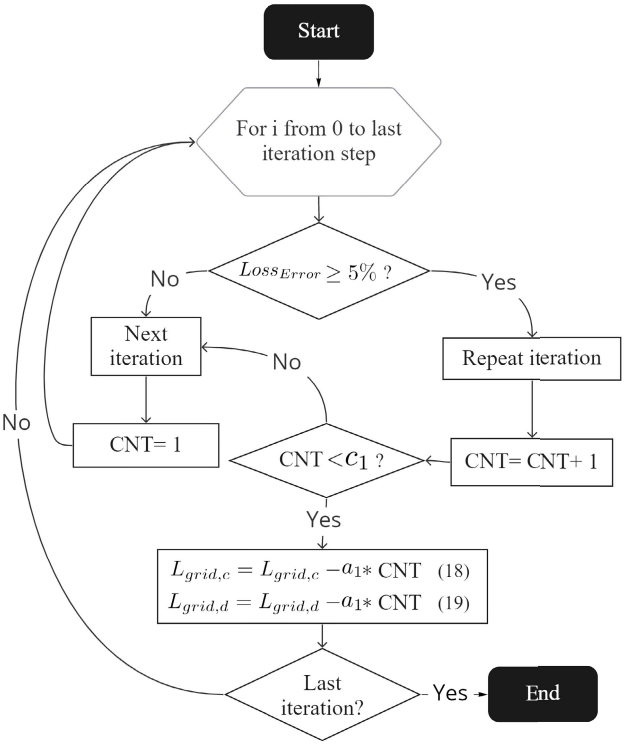

FIGURE 2. Flowchart of the losses control algorithm.

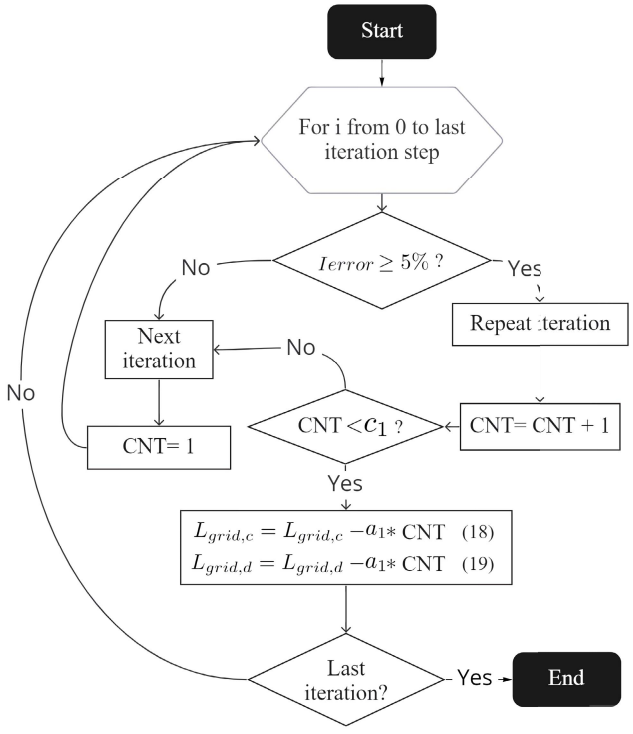

FIGURE 3. Flowchart of the congestion control algorithm.

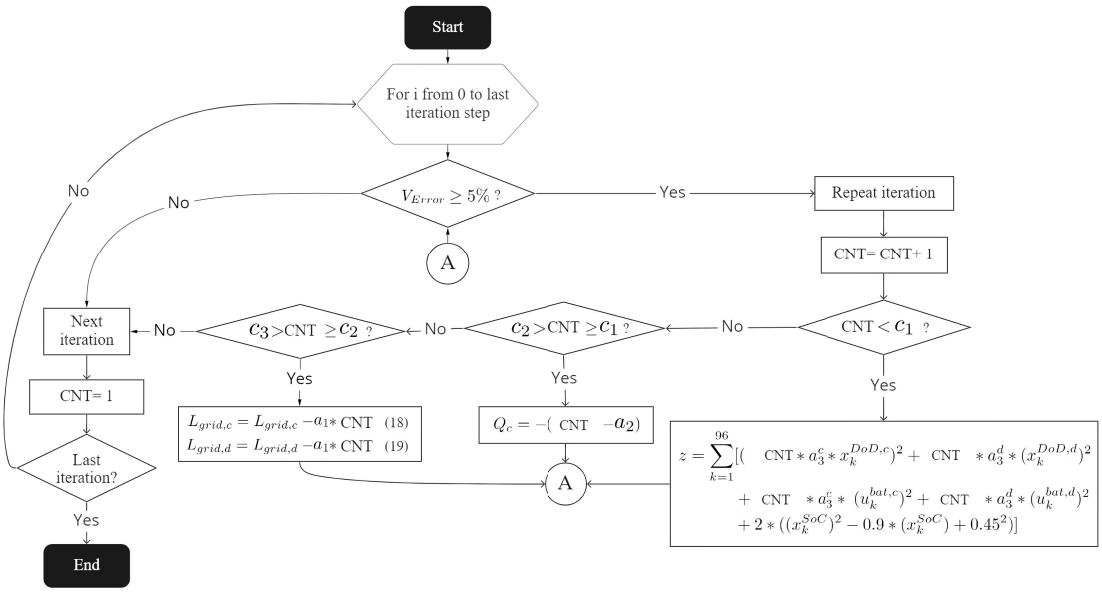

FIGURE 4. Flowchart of the voltage control algorithm.

respect to the case without the ACESS, the algorithm repeats the iteration that generates the error by gradually decreasing the grid participation limits to force a larger power contribution of the ACESS in the dispatch until reaching the point where the losses are decreased, or until the storage system cannot deliver more power. At this point, the algorithm advances to the next iteration having reduced the error as much as possible.

$$Loss_{Error} = 100\% * \frac{Loss_{Base} - Loss_{Present}}{Loss_{Base}} \tag{20}$$

3) CONGESTION REDUCTION CONTROL STRATEGY

The congestion control strategy, shown in Fig. 3, works in a similar way as the losses control strategy, but instead of focusing on the total losses of the system, it analyzes the currents flowing through the lines, always trying to reduce the highest current detected in any line of the system, as long as it is higher than the value calculated in the base case. Thus, the error parameter that modifies (18) and (19), calculated in (21), is the maximum current flowing through a system's line with respect to the current of the same line in the base case. By the nature of the ACESS, the moments when the batteries are charging are perceived by the network as a load. Therefore, the algorithm charges the ACESSs at times of low demand, so that the increase in current does not significantly affect the loading of the lines and, at times of high demand, the algorithm discharges the ACESS to achieve a congestion reduction.

$$I_{Error} = 100\% * \frac{I_{Base} - I_{Present}}{I_{Base}} \tag{21}$$

4) VOLTAGE CONTROL STRATEGY

The voltage control strategy implies several changes to the MPC described in Section II-A, because it requires modifying the objective function, including a new constraint for reactive power, and modifying the network participation limits (18) and (19) using the voltage error in (22). These modifications and the details of the voltage control strategy are described in the flowchart of Fig. 4

$$V_{Error} = 100\% * \frac{V_{Base} - V_{Present}}{V_{Base}} \tag{22}$$

The voltage control algorithm in Fig. 4 attempts to keep the voltage at all nodes of the system, for each iteration of the power flow, between 0.95 and 1.05 p.u. If the voltage error calculated in each iteration with respect to 1 p.u. is higher than 5%, the algorithm tries the following actions: first, it changes the weights of the objective function; second, it injects or absorbs reactive power using the ACESS; and third, it varies the limits of network participation in the dispatch. After this, the iteration with the best performance is saved and passed to the next step.

III. ALGORITHM IMPLEMENTATION

A. STUDY CASES: CONTROL STRATEGIES APPLIED TO THE IEEE 34-BUS FEEDER

The IEEE 34-bus feeder [20] in Fig. 5 is proposed as a test system for the different control strategies described in Section II. Since this is a system with static demand values, it was decided to apply the residential demand curve for MV systems provided by CIGRE [21], where 24 hours of energy consumption are shown as a function of a percentage of nominal apparent power. Additionally, the peak power of this system was reduced to one-fifth, since the original load of this system did not allow the correct operation of the proposed ACESS sizes. Since the MPC has a forecast horizon of 24 hours, the original 24-hour CIGRE curve was repeated to complete a 48-hour load curve, as shown in Fig. 6.

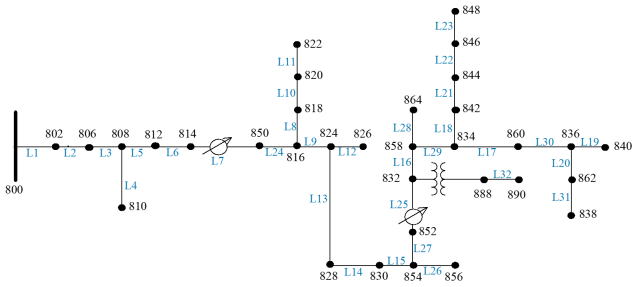

FIGURE 5. IEEE 34-node test system.

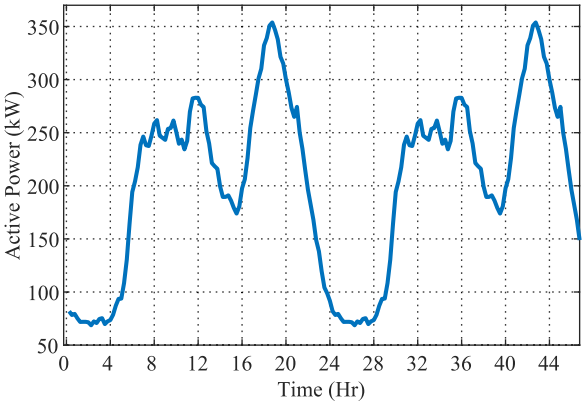

FIGURE 6. Demand curve used in the study cases.

In order to have a comparative basis for each control strategy, a power flow is run for each time step with no ACESS connected to the system, modifying the total system's loading to 80%, 100% and 120%, and extracting voltages, currents and losses at each node and line. Then, this base case is compared with three ACESS of 500 kWh, 1000 kWh and 1500 kWh following the peak saving, losses control and congestion reduction strategies. All these results set up Scenario 1. However, since the calculated dispatch for the proposed conditions in Scenario 1 is the same for the peak shaving, losses control and congestion reduction strategies, a second scenario is proposed for the last two strategies, assuming a total system's loading of 130% for an ACESS of 1500 kWh. Moreover, for the voltage control scheme, a total system's loading of 120% and a 2000 kWh ACESS is assumed. These parameters configure Scenario 2.

The parameters that are used in each control strategy are defined as follows: in the case of peak shaving, L_{grid}^{psl} in (18) and (19) is set to 240 kW. Also, for the losses and congestion control strategies depicted in Figs. 2 and 3, counter limit $c_1 = 15$, and $a_1 = 1.25$. Finally, for the voltage control algorithm of Fig. 4, $c_1 = 15$, $c_2 = 30$, $c_3 = 50$, $a_1 = 1.25$, $a_2 = c_2 = 30$, and $a_3 = 2$.

Furthermore, since the complementarity constraint (14) cannot be solved initially by a linear solver, the MPEC (Mathematical Programs with Equilibrium Constraint) extension for Pyomo [16] is used to convert this constraint to a simple disjunctive form by applying the Big-M or Convex Hull method, which can be easily interpreted by a linear solver.

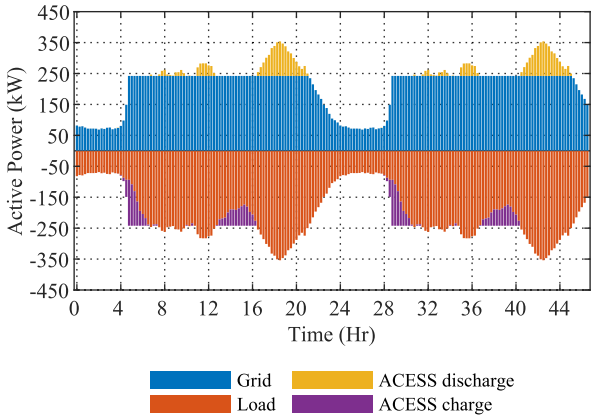

FIGURE 7. Power dispatch for different ACESSs following the peak shaving control strategy.

Finally, as a way to solve the power flows in each iteration, the py-dss-interface package [22] is used, which serves to execute and modify any OpenDSS script from the main Python code and extract the relevant results (currents, voltages, or losses), allowing to apply the control strategies to multinode systems and check their effect in each iteration.

B. HARDWARE AND SOFTWARE SPECIFICATIONS

The control strategies explained previously were implemented in Python 3.8.5 and were run on a laptop PC with Intel Core i5 9300H processor and 16 GB RAM. Power flow simulations were obtained from OpenDSS 9.3.0.1 [23], and the optimization problems described in Section II were coded in Pyomo 5.7.3 [16] and solved with CPLEX 20.1.0 [17]. Finally, for the ease of interfacing the optimization routines and power flow calculations in OpenDSS, the py-dss-interface 1.0.2 [22] was used, which allowed modifying existing scripts and extracting power flow results.

IV. RESULTS AND DISCUSSION

A. PEAK SHAVING CONTROL STRATEGY

Figure 7 presents the dispatch results of the peak shaving algorithm applied to three different ACESS, located at node 838, with capacities of 500 kWh, 1000 kWh and 1500 kWh. In Fig. 7, the yellow and purple bars represent the charging and discharging of the ACESS, respectively, the red bars denote the total system's demand, and the blue bars describe the network contribution to the system. The peak shaving algorithm flattens the grid participation curve by discharging the battery when the demand is over the 240 kW threshold, contributing to feed the surplus of peak consumption. From the point of view of energy demand, it can be observed in Fig. 7 that, when the load is below the 240 kW threshold, the ACESS is charged at the difference between 240 kW and the current load if the MPC considers it necessary. This means that, in those time intervals, the ACESS is recharged, achieving the effect of flattening the demand curve from the grid point of view.

Figure 8 shows the effect of the peak shaving strategy on SoC for the 500 kWh, 1000 kWh, and 1500 kWh ACESSs

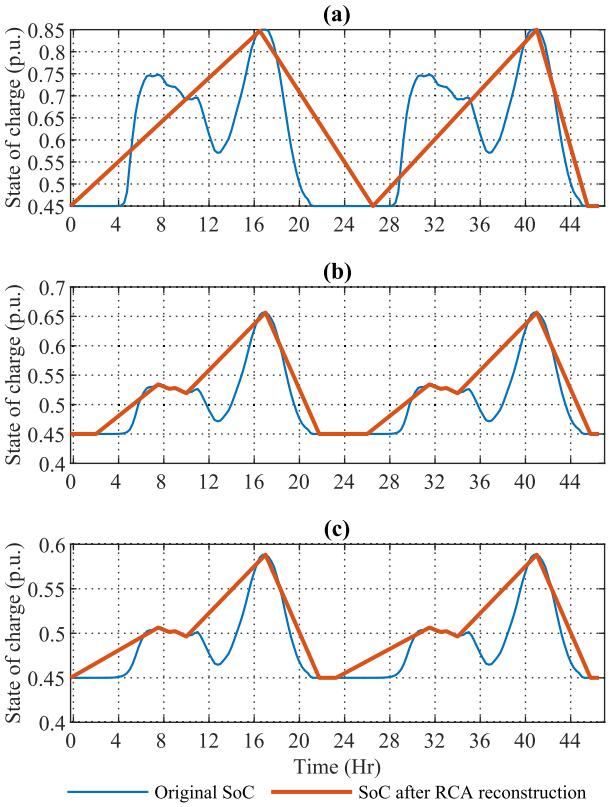

FIGURE 8. SoC reconstruction by RCA for different ACESS capacities following the peak shaving control strategy: (a) 500 kWh, (b) 1000 kWh, and (c) 1500 kWh.

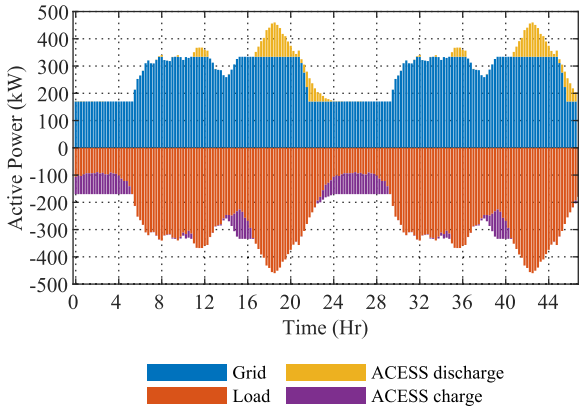

FIGURE 9. Power dispatch for a 1500 kWh ACESS following the losses control strategy.

and the reconstruction carried out by the RCA, corresponding to A, B and C, respectively. In can be seen that, at a lower storage capacity, the variation in the SoC is higher. This result is expected because the 500 kWh ACESS, compared to the 1000 kWh and 1500 kWh ACESSs, has to deliver a higher proportion of its stored energy to cover the peak demand. Considering that SoC limits were set between 0.2 p.u. and 0.85 p.u., the maximum energy that can be delivered continuously, in this case, is 65% of the total storage capacity [24]. Note that the 500 kWh system reaches the upper bounds at

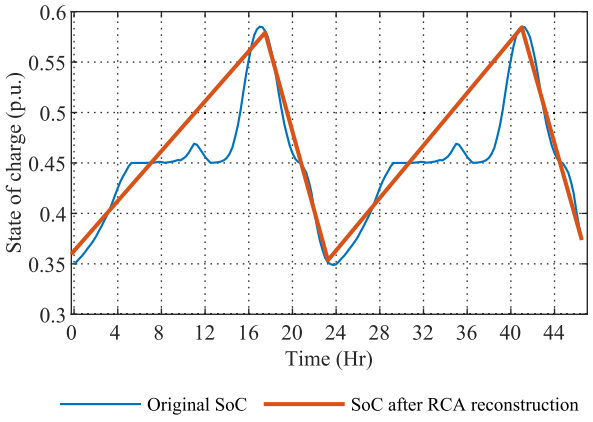

FIGURE 10. SoC reconstruction by RCA for a 1500 kWh ACESS following the losses control strategy.

TABLE 1. Losses control strategy results for Scenario 1.

System's Loading	ACESS capacity	500 kWh	1000 kWh	1500 kWh
80%	Losses reduction	12.78%	12.78%	12.78%
	Standard deviation	0.01%	0.01%	0.01%
100%	Losses reduction	14.2%	14.2%	14.2%
	Standard deviation	0.01%	0.01%	0.01%
120%	Losses reduction	15.1%	15.1%	15.1%
	Standard deviation	0.01%	0.01%	0.01%

the times of the highest demand, while the other two ACESSs remain closer to their initial SoC value of 0.45 p.u.

B. LOSSES CONTROL STRATEGY

Tests were carried out by placing the ACESS in all the nodes of the system for the three available storage capacities, i.e., 500 kWh, 1000 kWh, and 1500 kWh, and with three percentages of total system's loading, i.e., 80%, 100%, and 120%. The summary of the results of the line losses control algorithm for these tests is shown in Table 1. Note that, in the case of the IEEE 34 node system, neither the location nor the capacity of the ACESS affects significantly the reduction in losses. In the case of the location of the ACESS, a standard deviation of 0.01% in losses reduction was obtained for all tests, which means that the results of this table can be extrapolated to all the nodes of the system. In the case of the storage capacity, the losses reduction is the same for each loading condition, as expected, since the energy dispatch is the same for all ACESS capacities and only the SoC varies, as explained in Section IV-A. It was also observed that the only factor that affects the losses control strategy is the total loading, since in all cases the losses in the system are reduced, and this reduction is higher as loading increases, going from 12.78% to 15.1% losses reduction for the 80% and 120% loading cases.

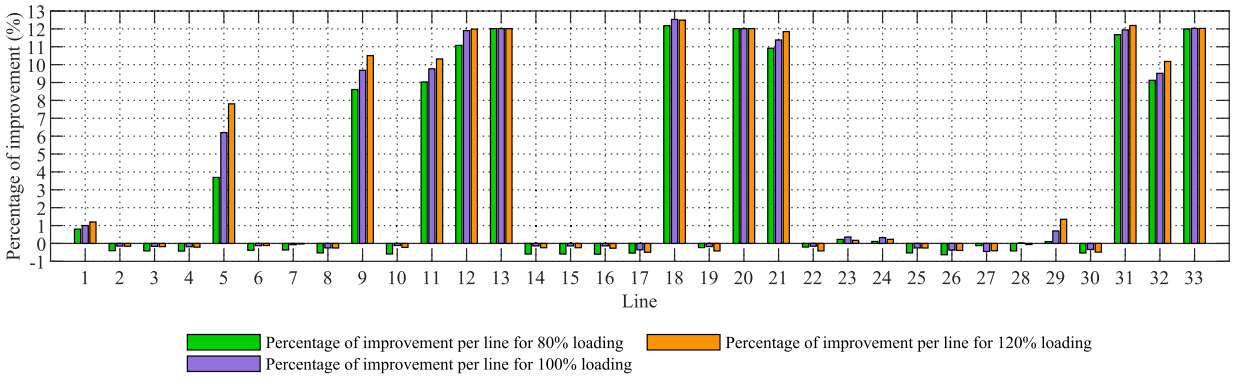

FIGURE 11. Summary of congestion control algorithm results on IEEE 34-bus feeder lines for 80%, 100% and 120% system's loading in Scenario 1.

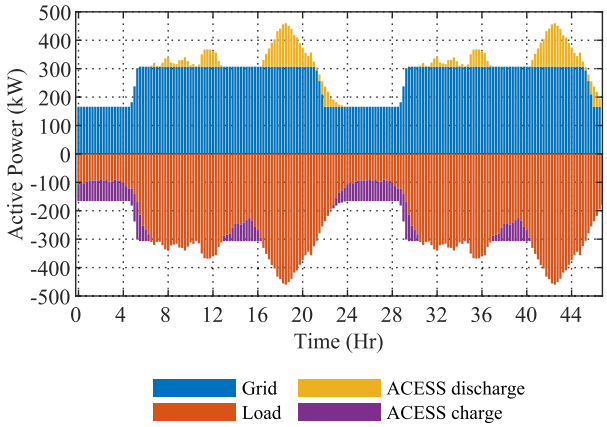

FIGURE 12. Power dispatch for a 1500 kWh ACESS following the congestion control strategy in Scenario 2.

As the dispatch for the given conditions did not change, a second scenario is proposed in order to see how the change of the constraints (18) and (19) affects the dispatch. In this scenario, a total loading of 130% is applied for the 1500 kWh ACESS. The dispatch results can be seen in Fig. 9, and the corresponding SoC in Fig. 10. In this case, it is observed that constraint (19) is decreased down to 170 kW, and constraint (18) is increased up to 334 kW. This brings the effect of charging the ACESS between 0 h to 5 h, and from 24 h to 29 h, allowing to cover part of the peak that occurs from 21 h to 24 h, and from 45 h to 46 h, by discharging the ACESS. The net effect of these control actions is a reduction of losses for the total dispatch of 15.41%.

C. CONGESTION CONTROL STRATEGY

Figure 11 shows the summary of congestion results on each of the IEEE 34-bus test system lines for the calculated 48-hour window. In this case, the BESS is located at node 838 because of its distant position with respect to the header node. Thus, Fig. 11 shows the average percentage of improvement for the 48 hours of the calculated dispatch. This is because the ACESS needs to consume or deliver energy in different moments, which means that at some times of the day, when the ACESS consumes energy, some lines will be more congested. However, after 48 hours of ACESS charging and discharging, it is observed a decrease in congestion at times when the battery delivers stored energy, which is more significant than the congestion it generates at times of low demand. This occurs because the MPC algorithm is programmed to encourage battery charging at low demand times, even if congestion increases, as it does not have a significant effect on the system. The opposite occurs at times of higher demand, when the ACESS is discharged, which is perceived from the header node as a reduction in the demand.

Since the initial dispatch with the proposed conditions is the same as the obtained in the peak shaving control strategy, an additional scenario is proposed for the losses control strategy in order to see the change in constraints (18) and (19), and the dispatch. In this new scenario, a total system loading of 130% is applied to the system, and an ACESS of 1500 kWh is used for reducing line congestions. The dispatch results of this new scenario can be found in Fig. 12, and the corresponding SoC in Fig. 14. In this case, it is observed that the constraint (19) is decreased down to 166 kW, and the constraint (18) increased up to 307 kW, which allows charging the battery between 0 h to 6.25 h, and from 24 h to 30.25 h. This dispatch fully covers the peak demand from 16.5 h to 24 h, and between 40.5 h and 47 h, resulting in the current reduction presented in Fig. 13. This figure shows a current's decrease of 0.5% with respect to the total system's loading of 120%; however, this case also shows that the higher the system's loading, the better the effectiveness of the losses control strategy.

D. VOLTAGE CONTROL STRATEGY

In the case of the voltage control strategy, tests carried out without the ACESS determined that the largest voltage drops occurred at node 890, where the storage system was finally located to assess this algorithm. Moreover, the system was overloaded to 120% of the nominal value to increase voltage deviations so that the strategy could be easily tested. Finally, the storage capacity of the ACESS for this case is 2000 kWh.

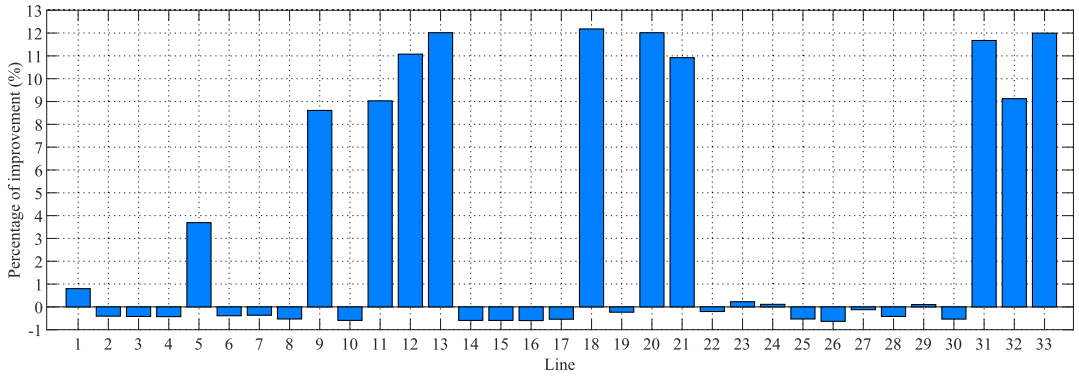

FIGURE 13. Summary of congestion control algorithm results on IEEE 34-bus feeder lines for 150% loading in Scenario 2.

TABLE 2. Degradation results for SoCs in Fig. 8.

Control strategy	Peak shaving, Losses, Congestion					
Capacity	500 kWh		1000 kWh		1500 kWh	
Variables	Cycle lifetime	% of Degradation	Cycle lifetime	% of Degradation	Cycle lifetime	% of Degradation
Lower currents lifetime estimation	3716.1	7.1	5507.4	-37.68	4819	-20.47
Average lifetime	1728.0	46	4458.7	-11.47	4997.7	-24.94
Highest currents lifetime estimation	2159.6	56.8	3534.8	11.63	5413	-35.33

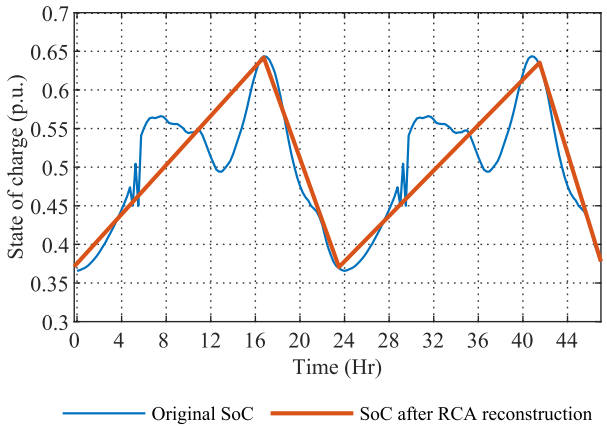

FIGURE 14. SoC reconstruction by RCA for a 1500 kWh ACESS following the congestion control strategy in Scenario 2.

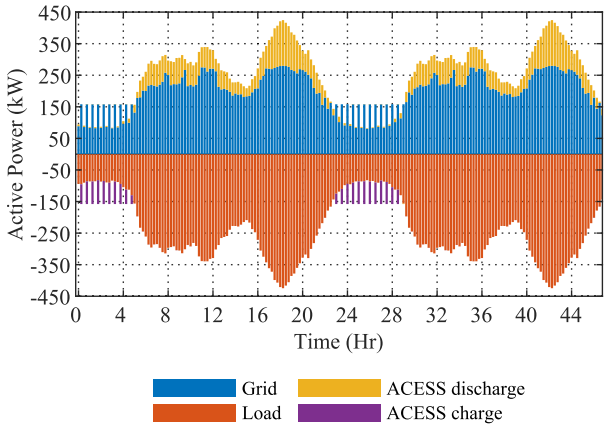

FIGURE 15. Power dispatch for a 2000 kWh ACESS following the voltage control strategy.

The resulting dispatch for the voltage control strategy is shown in Fig. 15, where variations can be observed in the

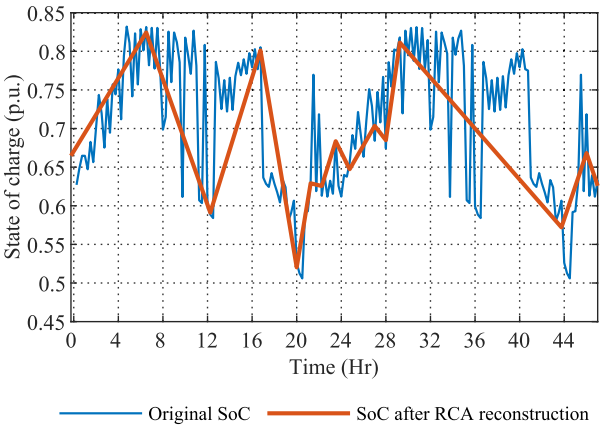

FIGURE 16. SoC reconstruction by RCA for a 2000 kWh ACESS following the voltage control strategy.

grid contributions from 5 h to 23 h, and from 30 h to 47 h. This is due to overvoltages during those periods that cannot be corrected through the change in the objective function coefficients or reactive power consumption, so that the grid limits are changed to allow the ACESS delivering a greater amount of energy in those specific moments. This means a grid participation that varies from 180 kW to 275 kW, so that the difference between these values and the demand is supplied by the ACESS, as seen in the variation of the ACESS SoC in Fig. 16. Note that the peaks observed in the dispatch correspond to the peaks existing in the SoC, which implies that the ACESS assumes such variations to try to improve the voltage.

Figure 17 shows the overvoltage values that were improved by more than 0.1% with respect to the initial voltage value and the 15-min sample at which these overvoltages occurred. Only these values are shown since there are 187 time steps

TABLE 3. Degradation results for SoC reconstructed in Figs. 10, 14, 16.

Control strategy	Losses		Congestion		Voltage	
Capacity	1500 kWh		1500 kWh		2000 kWh	
Variables	Cycle lifetime	% of Degradation	Cycle lifetime	% of Degradation	Cycle lifetime	% of Degradation
Lower currents lifetime estimation	3044.1	23.9	3.3625	15.94	3182.3	20.4437
Average lifetime	3018.7	24.53	3.3445	16.3	2703.8	32.4046
Highest currents lifetime estimation	2990.7	25.23	3.3196	17.01	1465.0	63.3754

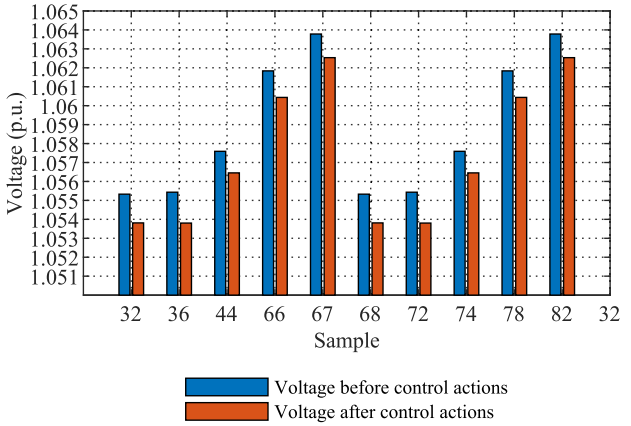

FIGURE 17. Voltage behavior at node 890 in selected samples.

recorded, and in most of them there are no voltage problems. Note that in most cases, the voltage manages to drop to a value equal or close to 1.05 p.u. However, for points such as 32, 36, 68 or 72, even though the improvement in voltage is around 0.15%, it is not enough to drop the voltage to 1.05 p.u. The algorithm continues because another modification on the conditions of the optimization problem ends up leading to the non-convergence of the power flow.

E. DEGRADATION RESULTS

To estimate the degradation of the different ACESSs that were used in the previous study cases, the RCA proposed in [25] and implemented for other ACESS in [26] was applied. In order to run the RCA algorithm, the ACESS SoC resulting from the MPC was used as input. Table 2 describes the results of the RCA sorted by control strategy, ACESS capacity, degradation percentage, and remaining service lifetime in cycles according to the SoCs in Fig. 8. Also, Table 3 shows the results corresponding to the RCA reconstructions in Figs. 10, 14 and 16. In some cases, negative degradation percentages are obtained, which is interpreted as the remaining service lifetime if the usage is higher than the one originally indicated by the manufacturer. By contrast, positive degradation percentages indicate a reduction in service lifetime and a lower number of remaining cycles compared to manufacturer's specifications if that usage pattern is maintained.

From the results listed in Table 2, it is possible to observe that, for most of the control strategies, the degradation of the storage system decreases as the storage capacity increases. This is expected because, as observed in Fig. 8, for the same dispatch, a higher storage capacity implies a lower variation of SoC, and therefore, a lower degradation estimated with RCA. However, Table 3 shows that, even though there is 1500 kWh storage capacity, it is possible to degrade the battery if the input SoC presents high variations, as it is the case in Figs. 10, 14 and 16, where average degradation values of 24.5%, 16.3%, and 32.4% are found for the losses, congestion and voltage control strategies, respectively.

V. CONCLUSION

This study presented the conceptual approach and simulation of four control strategies (peak shaving, losses control, congestion control, and local voltage control) applied to an ACESS in a modified IEEE 34-bus feeder. The study was based on the use of an MPC as a way to estimate the necessary battery charging and discharging actions, taking into account the future conditions of the demand and the system in a 24-hour prediction window. In the case of the peak shaving algorithm, successful dispatch was obtained for three different ACESS capacities, showing a maximum peak reduction of 31.54%. For the losses and congestion control algorithms, the reduction of losses and currents was estimated in terms of the base case without ACESS in the system, obtaining a maximum reduction of 15.4% and 12.44% of losses and congestion, respectively. In the case of voltage control algorithm, improvements between 0.1% and 0.15% were obtained with respect to the voltage increases seen in the base case, although several times the ACESS failed to place the voltage within the 0.95-1.05 p.u. band because of an insufficient active and reactive power control capacity. Finally, the degradation of the 3 ACESSs under different control strategies was estimated with the RCA, showing that voltage control strategy produces the highest degradation, reaching a service lifetime reduction of up to 63.4% in the worst case scenario and, in the best case scenario for the rest of control strategies, a service lifetime extension of up to 35.3%. Future work will focus on improving the local voltage control strategy and analyzing other ancillary services with ACESSs that are typically seen in BESSs of high capacity, such as primary frequency control.

REFERENCES

[1] H. Nagpal, I.-I. Avramidis, F. Capitanescu, and A. G. Madureira, "Local energy communities in service of sustainability and grid flexibility provision: Hierarchical management of shared energy storage," *IEEE Trans. Sustain. Energy*, vol. 13, no. 3, pp. 1523–1535, Jul. 2022.

[2] T. AlSkaif, W. Schram, G. Litjens, and W. van Sark, "Smart charging of community storage units using Markov chains," in *Proc. IEEE PES Innov. Smart Grid Technol. Conf. Eur. (ISGT-Europe)*, Sep. 2017, pp. 1–6.

[3] C. P. Mediwaththe, E. R. Stephens, D. B. Smith, and A. Mahanti, "Competitive energy trading framework for demand-side management in neighborhood area networks," *IEEE Trans. Smart Grid*, vol. 9, no. 5, pp. 4313–4322, Sep. 2018.
[4] B. P. Koirala, E. van Oost, and H. van der Windt, "Community energy storage: A responsible innovation towards a sustainable energy system?" *Appl. Energy*, vol. 231, pp. 570–585, Dec. 2018.
[5] (2021). U.S. Energy Information Administration (EIA). *Battery Storage in the United States: An Update on Market Trends*. [Online]. Available: https://www.eia.gov/analysis/studies/electricity/batterystorage/pdf/battery_storage_2021.pdf
[6] H.-C. Jo, G. Byeon, J.-Y. Kim, and S.-K. Kim, "Optimal scheduling for a zero net energy community microgrid with customer-owned energy storage systems," *IEEE Trans. Power Syst.*, vol. 36, no. 3, pp. 2273–2280, May 2021.
[7] R. H. Byrne, T. A. Nguyen, D. A. Copp, B. R. Chalamala, and I. Gyuk, "Energy management and optimization methods for grid energy storage systems," *IEEE Access*, vol. 6, pp. 13231–13260, 2017.
[8] D. Parra, M. Swierczynski, D. I. Stroe, S. A. Norman, A. Abdon, J. Worlitschek, T. O'Doherty, L. Rodrigues, M. Gillott, X. Zhang, and C. Bauer, "An interdisciplinary review of energy storage for communities: Challenges and perspectives," *Renew. Sust. Energ. Rev.*, vol. 79, pp. 730–749, 2017.
[9] M. Koller, T. Borsche, A. Ulbig, and G. Andersson, "Defining a degradation cost function for optimal control of a battery energy storage system," in *Proc. IEEE Grenoble Conf.*, Jun. 2013, pp. 1–6.
[10] N. Jayasekara, M. A. S. Masoum, and P. J. Wolfs, "Optimal operation of distributed energy storage systems to improve distribution network load and generation hosting capability," *IEEE Trans. Sustain. Energy*, vol. 7, no. 1, pp. 250–261, Jan. 2016.
[11] R. Hemmati, H. Saboori, and M. A. Jirdehi, "Stochastic planning and scheduling of energy storage systems for congestion management in electric power systems including renewable energy resources," *Energy*, vol. 133, pp. 380–387, Aug. 2017.
[12] E. Dehnavi, F. Aminifar, and S. Afsharnia, "Congestion management through distributed generations and energy storage systems," *Int. Trans. Electr. Energy Syst.*, vol. 29, no. 6, pp. 1–12, 2019.
[13] S. Dehbozorgi, A. Ehsanifar, Z. Montazeri, M. Dehghani, and A. Seifi, "Line loss reduction and voltage profile improvement in radial distribution networks using battery energy storage system," in *Proc. IEEE 4th Int. Conf. Knowl.-Based Eng. Innov. (KBEI)*, Dec. 2017, pp. 215–219.
[14] A. Zecchino, Z. Yuan, F. Sossan, R. Cherkaoui, and M. Paolone, "Optimal provision of concurrent primary frequency and local voltage control from a BESS considering variable capability curves: Modelling and experimental assessment," *Electr. Power Syst. Res.*, vol. 190, Jan. 2021, Art. no. 106643.
[15] Y. Wang, K. T. Tan, X. Y. Peng, and P. L. So, "Coordinated control of distributed energy-storage systems for voltage regulation in distribution networks," *IEEE Trans. Power Del.*, vol. 31, no. 3, pp. 1132–1141, Jun. 2016.
[16] W. E. Hart, C. D. Laird, J.-P. Watson, D. L. Woodruff, G. A. Hackebeil, B. L. Nicholson, and J. D. Siirola, *Pyomo-Optimization Modeling in Python*, vol. 67. Cham, Switzerland: Springer, 2017.
[17] *V12. 8: User's Manual for CPLEX*, IBM ILOG CPLEX, Int. Bus. Mach. Corp., Armonk, NY, USA, 2017, p. 596.
[18] S. V. Giannoutsos and S. N. Manias, "A cascade control scheme for a grid connected battery energy storage system (BESS)," in *Proc. IEEE Int. Energy Conf. Exhib. (ENERGYCON)*, Sep. 2012, pp. 469–474.
[19] N. Shidore, T. Bohn, M. Duoba, H. Lohse-Busch, and P. Sharer, "PHEV 'all electric range' and fuel economy in charge sustaining mode for low SOC operation of the JCS VL41M Li-ion battery using battery HIL," in *Proc. electric vehicle Symp.*, vol. 23, 2007, pp. 2–5.
[20] (1992). IEEE Power System Analysis, Computing and Economics Committee. *IEEE 34 Node Test Feeder*. [Online]. Available: https://cmte.ieee.org/pes-testfeeders/resources/
[21] K. Strunz et al., "Benchmark systems for network integration of renewable and distributed energy resources—CIGRE task force C6.04.02," CIGRE, Paris, France, Tech. Rep. 575, Apr. 2014.
[22] P. Radatz, E. Viana, and R. Pilar, *Py-DSS-Interface Documentation*, 1st ed. 2021. [Online]. Available: https://py-dss-interface.readthedocs.io/en/latest/readme.html
[23] R. Dugan, D. Montenegro, and A. Ballanti, *The Open Distribution System Simulator (OpenDSS) Reference Guide*, 9th ed. Palo Alto, CA, USA: Electric Power Research Institute, 2020.
[24] T. Terlouw, T. AlSkaif, C. Bauer, and W. van Sark, "Multi-objective optimization of energy arbitrage in community energy storage systems using different battery technologies," *Appl. Energy*, vol. 239, pp. 356–372, Apr. 2019.
[25] V. Muenzel, J. de Hoog, M. Brazil, A. Vishwanath, and S. Kalyanaraman, "A multi-factor battery cycle life prediction methodology for optimal battery management," in *Proc. ACM 6th Int. Conf. Future Energy Syst.*, 2015, pp. 57–66.
[26] H. Yepes-Fernández, M. Restrepo, and A. Arango-Manrique, "Lifetime degradation study of batteries operating as community energy storage systems," in *Proc. IEEE Andescon*, Oct. 2022, pp. 1–6.

HERNÁN YEPES-FERNÁNDEZ (Student Member, IEEE) received the B.E. degree in electrical engineering from Universidad del Norte, Barranquilla, Colombia, in 2021, where he is currently pursuing the M.Sc. degree in electrical engineering. His research interests include storage systems and smart grids.

MAURICIO RESTREPO (Member, IEEE) received the Diploma degree in electrical engineering from Universidad Pontificia Bolivariana, Medellin, Colombia, in 2006, and the Ph.D. degree in electrical and computer engineering from the University of Waterloo, Waterloo, ON, Canada, in 2017. He is currently an Assistant Professor at Universidad del Norte, Barranquilla, Colombia. His research interests include smart grids, transportation electrification, and power electronics.

ADRIANA ARANGO-MANRIQUE (Member, IEEE) received the B.E. degree in electrical engineering and the M.Sc. and Ph.D. degrees in engineering from the Universidad Nacional de Colombia at Manizales, Colombia, in 2008, 2010, and 2018, respectively. She is currently a full-time Professor with the Universidad del Norte, Barranquilla, Colombia. She is also working with the GISEL Research Group. Her research interests include demand response, electricity markets, energy transitions, and power systems.